Phase Characterization and Mechanical and Flame-Retarding Properties of Nano-$CaSO_4$/Polypropylene and Nano-$Ca_3(PO_4)_2$/Polypropylene Composites

S. Mishra, Arindam Mukherji

Department of Chemical Technology, North Maharashtra University, Jalgaon 425001, P.O. Box 80, Maharashtra State, India

Received 7 June 2005; accepted 9 October 2005
DOI 10.1002/app.23954
Published online in Wiley InterScience (www.interscience.wiley.com).

ABSTRACT: An *in situ* deposition approach was used for the synthesis of nano-$CaSO_4$ and nano-$Ca_3(PO_4)_2$. The nanosize particles were confirmed with an X-ray diffraction technique. Composites of polypropylene (PP) with 0.1–0.5 wt % nano- or commercial $CaSO_4$ or nano-$Ca_3(PO_4)_2$ were prepared. The transition from the α phase to the β phase was observed for 0.1–0.3 wt % nano-$CaSO_4$/PP and nano-$Ca_3(PO_4)_2$/PP composites. This was confirmed by Fourier transform infrared. A differential scanning calorimetry analysis was carried out to determine the thermal behavior of the nanocomposites with increasing amounts of the nano-$CaSO_4$ and nano-$Ca_3(PO_4)_2$ fillers. Increases in the tensile strength and Young's modulus were observed up to certain loading and were followed by a decrease in the tensile strength. A continuous decrease in the elongation at break (%) was also observed for commercial $CaSO_4$ and larger nano-$Ca_3(PO_4)_2$. A decrease in the mechanical properties after a certain loading might have been due to the agglomeration and phase transition of PP in the composites. J Appl Polym Sci 103: 670–680, 2007

Key words: flame retardence; mechanical properties; nanoparticles; poly(propylene) (PP)

INTRODUCTION

In the past few years, new methodologies have been developed to prepare materials containing organic and inorganic fillers. A uniform distribution of small particles within the polymer matrix is an important factor for promoting strong interfacial adhesion between the matrix and nanofillers. Such reinforcement of a single phase has to produce new systems called hybrids or nanocomposites. Hybrid composites exhibit drastic improvements in the superconductivity, magnetism, thermal stability, and mechanical properties because of the high surface area of the nanoparticles and their enormous interfacial adhesion with the virgin matrix.[1]

Many researchers have extensively worked on clay–polymer systems.[2–6] In thermoplastic-based (intercalated or exfoliated) nanocomposites, the ultimate strength of the material can vary, depending on the nature of the interaction between the matrix and the filler. Synthetic mineral nanofillers such as nano-$Mg(OH)_2$, nano-$CaCO_3$, nano-ZnO, and nano-TiO_2 are different from mineral clay because of their treatment methods, commercial aspects, problems in handling, and agglomeration in polymer matrices. Researchers have attempted different routes for the synthesis of mineral nanoparticles, which include mainly (1) sol–gel,[7] (2) microemulsion,[8] and (3) *in situ* deposition methods.[9] Of these methods, *in situ* deposition controls the matrix-mediated growth and morphology in the synthesis of materials.[10,11] In this method, the growth of phases is restricted to certain crystalline phases (α and β), in comparison with the large number of phases developed in normal solution precipitation. These restricted phases are responsible for drastic improvements in the mechanical properties of polymer nanocomposites. The shape and morphology of the nanoparticles are responsible for improvements in the mechanical properties of nanofilled composites; that is, nano-$CaCO_3$ is spherical, and $CaSO_4$ has a needlelike structure.[12] This article is a comparative study of the mechanical and flame-retarding performances of polypropylene (PP) composites filled with nano- or commercial $CaSO_4$ or nano-$Ca_3(PO_4)_2$.

EXPERIMENTAL

Materials

PP (grade 310367, Repol) with a melt flow index of 8.94 g/10 min and a density of 0.92 g/cc was pro-

This article was partially presented at Macro-2004, the International Conference on Polymers for Advanced Technologies (December 14–17, 2004, Thiruvananthapuram, India).

Correspondence to: S. Mishra (profsm@rediffmail.com).

Contract grant sponsor: Department of Science and Technology (New Delhi, India); contract grant number: SR/S-5/WM-31/2003.

Journal of Applied Polymer Science, Vol. 103, 670–680 (2007)

cured from Reliance Industries, Ltd. (India). Analytical grades of calcium chloride and ammonium sulfate, diammonium hydrogen phosphate, and poly(ethylene glycol) (PEG; molecular weight = 6000), procured from Qualigens India, Ltd. (Mumbai, India), were used for the synthesis of nanoparticles of calcium sulfate and calcium phosphate.

Nanoparticle and composite preparation with characterization

The nanoparticles were synthesized by a matrix-mediated growth technique;[11–18] the ammonium sulfate and ammonium phosphate were used in place of potassium carbonate to synthesize the calcium sulfate and calcium phosphate nanoparticles, respectively. PP granules and nanoparticles were premixed in different weight percentages in a Rheomix 600 mixer (Rheocord 900, Haake, Germany). The temperatures of the feed zone, compression zone, metering zone, and die were kept at 225, 225, 225, and 250°C, respectively. The die gap, screw diameter, and screw length were 1, 19.1, and 477.5 mm, respectively. The mixing was performed at 50 rpm for 10 min. The nanosizes were confirmed with an X-ray diffractometer (Rigaku, Tokyo, Japan) with an intensity of 0–6000 Cps and a diffraction angle of 0–35°. The particle sizes were determined with Scherrer's formula:[11,16,17]

$$\text{Particle size } (\text{Å}) = k\,\lambda/\Delta 2\theta\,\cos\,\theta \qquad (1)$$

where k is the order of reflection, λ is 1.542, θ is the diffraction angle, and $\Delta 2\theta$ is the full width at half-maximum. The particle sizes of the two different ratios (1 : 4 and 1 : 20) of PEG and calcium chloride were recorded as 12 and 22 nm for $CaSO_4$ and 13 and 24 nm for $Ca_3(PO_4)_2$, respectively.

Differential scanning calorimetry (DSC)

The crystallization behavior of the PP composites was recorded on a PerkinElmer differential scanning calorimeter (Perkin Elmer, Wellesley, MA). The crystallization was studied in the range of 50–250°C at a rate of 10°C/min in a nitrogen environment. Furthermore, to ensure complete melting, the sample was held for 1 min at 250°C and then cooled to 50°C at the same rate.

The crystallinity of virgin PP and its composites (C_i) was determined with the following relationship:

$$C_i = (\Delta H_f/\Delta H_s) \times 100 \qquad (2)$$

where ΔH_f is the heat of fusion of the PP polymer and ΔH_s is the heat of fusion of PP under standard conditions (i.e., 206.74 kcal/mol).

Optical microscopy analysis

Thin films of extruded samples were exposed for micrographs on an optical microscope (STM-5, RE-312, Olympus, Tokyo, Japan).

Mechanical properties

Tensile specimens of extruded sheets (according to ASTM D 628) were tested on a universal testing machine (model UT-2303, R&D Electronics, Mumbai, India). Testing was done at room temperature. Young's modulus and the elongation at break (%) were determined at a deformation speed of 5.00 cm/min. A mean value of five measurements was taken.

Flame retardancy

A flame-retardancy test was carried out in a flame tester (Prolific flammability tester, Noida, India) according to ASTM D 635. Each sample was clamped 85 mm above the horizontal screen so that it would not sag out to touch the screen. A free end was exposed to a specified gas flame for 30 s. The sample was clamped at a 45° angle to the flame tip. The time required for burning and the relative rate of burning were measured.[16]

Specific gravity

An analytical balance equipped with a stationary support for an immersion vessel above or below the balance pan was used for the specific gravity measurement. Corrosion-resistant wire for suspending the specimen and a sinker for a lighter specimen with a specific gravity of less than 1 were employed. A beaker was used as an immersion vessel. A test specimen of a convenient size was weighed in air, and then the specimen was suspended from a fine wire attached to the balance and completely immersed in distilled water. The weight of the specimen in water was determined (with the sinker). The specific gravity of the specimen was calculated as follows:

$$\text{Specific gravity} = a/(a + w) - b \qquad (3)$$

where a is the weight of the specimen in air, b is the weight of the specimen (with the sinker) and wire in water, and w is the weight of the totally immersed sinker and partially immersed wire.

RESULTS AND DISCUSSION

Fourier transform infrared (FTIR) characterization of the PP–$CaSO_4$ and PP–$Ca_3(PO_4)_2$ nanocomposites

Figure 1(a,b) shows the FTIR characterization of virgin PP and its nanocomposites. Drastic changes can

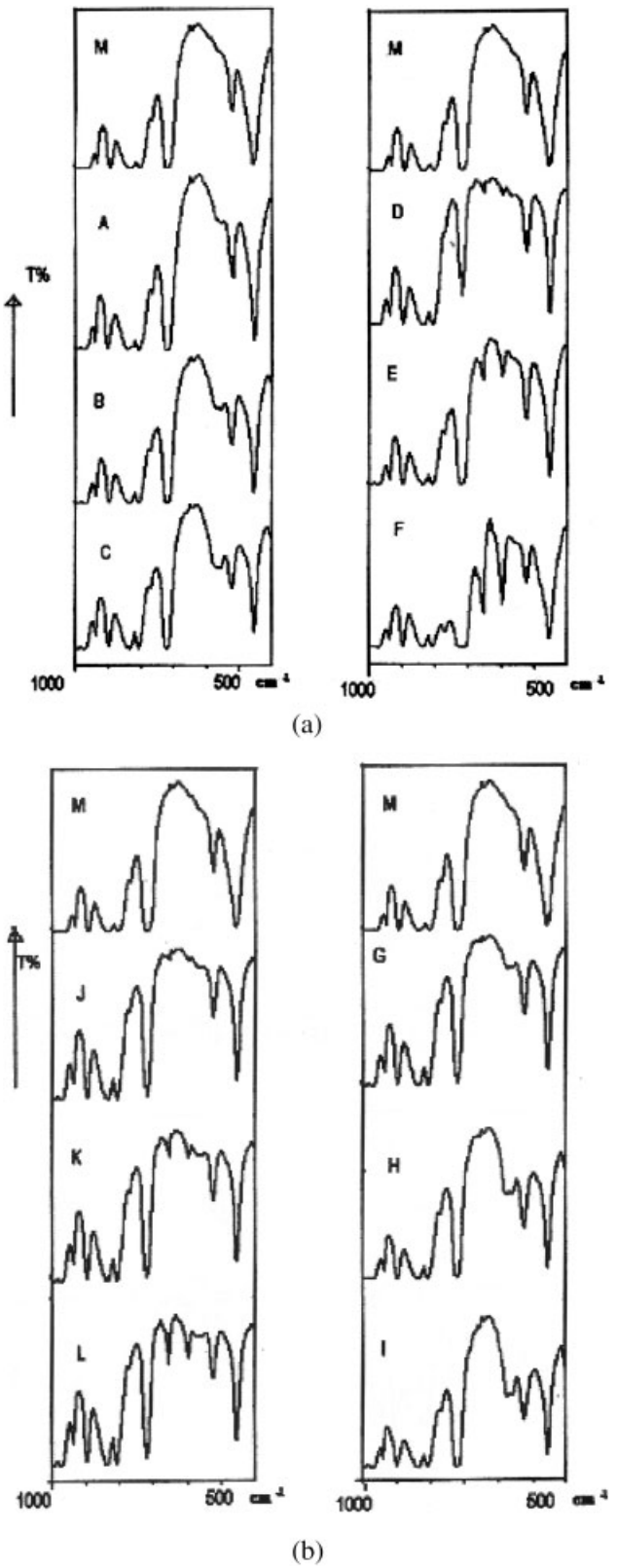

Figure 1 (a) FTIR spectra of 22-nm $CaSO_4$/PP composites [(A) 0.1, (B) 0.3, and (C) 0.5%] and 24-nm $Ca_3(PO_4)_2$/PP composites [(M) 0.0, (D) 0.1, (E) 0.3, and (F) 0.5%] and (b) FTIR spectra of 12-nm $CaSO_4$/PP composites [(J) 0.1, (K) 0.3, and (L) 0.5%] and 13-nm $Ca_3(PO_4)_2$/PP composites [(M) 0.0, (G) 0.1, (H) 0.3, and (I) 0.5%].

be observed in the FTIR peaks of the 500–1000-cm^{-1} region. The changes in the FTIR spectra of all $CaSO_4$ composites are appreciable in comparison with the $Ca_3(PO_4)_2$ composites. The bands obtained at 459.0, 528.5, 721.3, 773.1, and 970.1 cm^{-1} for virgin PP can be assigned to the α phase of virgin PP. After the addition of various weight percentages of nano-$CaSO_4$ and nano-$Ca_3(PO_4)_2$, the α phase changes to the β phase; hence, the β form is more prominent, as observed in the FTIR spectra. Different peaks can be observed with increasing weight percentages with a reduction in the nanosize and with changes in the structure of the nanofillers. In the case of nano-$CaSO_4$, a change in the IR range from 563 to 688 cm^{-1} can be observed upon the addition of 0.1–0.5 wt % of different nanosizes. New peaks have been recorded at 688, 661.5, and 599.8 cm^{-1} for the 0.5 wt % 12-nm $CaSO_4$ composite, and peaks at 563.2 and 644.2 cm^{-1} have appeared for 0.1 and 0.3 wt % 24-nm $CaSO_4$ composites. These peaks can be assigned to the β phase. In the case of 0.3 wt % 24-nm $Ca_3(PO_4)_2$, a new peak at 599.8 cm^{-1} can be observed. Similarly, new peaks have developed at 644.2 and 563 cm^{-1} for 0.1 and 0.3 wt % 13-nm $Ca_3(PO_4)_2$, respectively. Overall, at a certain weight percentage of filler addition, some new peaks develop, and subsequently depression in the same peaks can be observed upon the addition of a high weight percentage. This may be due to the orientation of molecules by intercalation and the disorientation of molecules by exfoliation due to the higher addition of fillers. The agglomeration of nanoparticles observed in the optical micrographs Figures 2 and 3 may also be a reason. PP molecules are exfoliated after the addition of a certain amount of a filler. This is supported by our earlier work,[17] in which the same results were observed. In this study, the weight percentage of exfoliation is 0.3. Radhakrishnan and Saujanya[11,15] and Wang et al.[19] reported the same kind of conclusion concerning the changes in the phases based on the X-ray diffraction and FTIR peaks at higher weight percentages of the loading of the nanofiller. Jog and Priya[20] studied the CF bending and CH twisting at different IR peaks of poly(vinylidene fluoride). They concluded that a possible increase in the mechanical properties was due to the changes in the phases from α to β through γ.

Effect of the nanoparticles on the thermal properties of the PP nanocomposites

Figures 4 and 5 show DSC thermograms of virgin PP and composites containing nano-$CaSO_4$ and nano-$Ca_3(PO_4)_2$ with various weight percentages of the fillers and a reduction in the nanosizes. In the case of $CaSO_4$ nanocomposites, the heat of fusion decreases with an increase in the weight percentage of the filler.

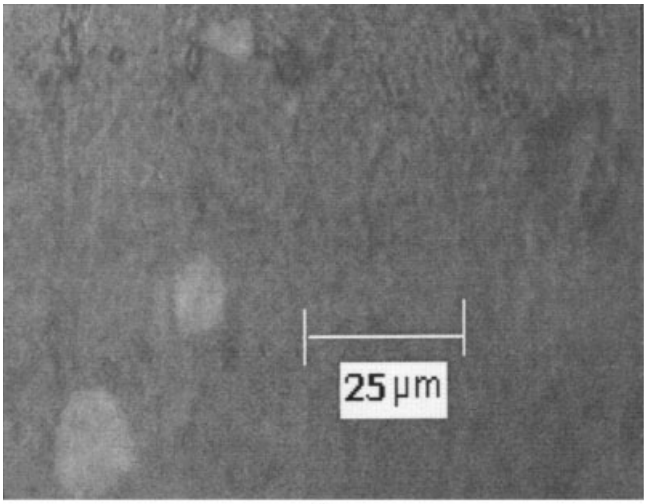

(a)

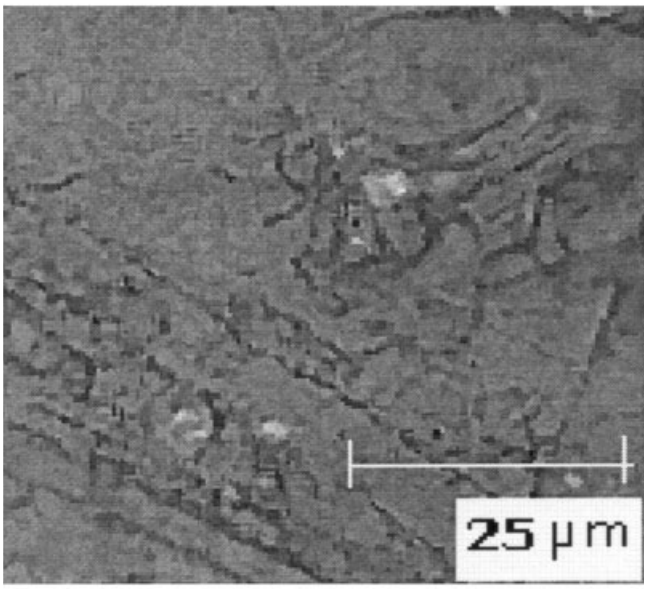

(b)

Figure 2 Optical micrographs (400×) of (a) a 0.1 wt % 12-nm $CaSO_4$/PP composite and (b) a 0.5 wt % 12-nm $CaSO_4$/PP composite.

A similar effect of the absorption of heat can also be observed for $Ca_3(PO_4)_2$ composites. Even in both cases, the absorption of heat energy increases with a reduction in the nanosize. This is due to a higher increase in the surface area of the nanoparticles. It has also been found that the structural effect of both kinds of nanoparticles shows a difference in the heat of absorption. $CaSO_4$ has a needlelike structure, and $Ca_3(PO_4)_2$ has a spherical structure. As shown in Table I, the $Ca_3(PO_4)_2$ composites show almost higher absorption in heat energy in comparison with the $CaSO_4$ composites. Details of DSC thermograms such as the peak temperatures and heat of fusion are listed in Table I. The melting point shows the marginal increase in the values; for example, virgin PP has a melting point of 162.16°C, and all the composites show melting points in the range of 162–163°C. As the addition of nanoparticles is very small (0.1–0.5 wt %), it is obvious that the melting temperature does not show any higher increase. The nanosize reduction also shows an effect on the crystallinity percentage (Table I). The crystallinity percentage decreases with a reduction in the nanosize.

Like FTIR spectra, the change in the α phase can also be observed prominently in the case of the additions of 0.3 wt % nano-$CaSO_4$ by the appearance of multiple melting peaks in the DSC thermograms. However, in the case of $Ca_3(PO_4)_2$, the multiple melting peaks are less, and this may by due to less change in the α phase to the β phase because of the lower aspect ratio of $Ca_3(PO_4)_2$ in comparison with that of $CaSO_4$.

Specific gravity

As shown in Figure 6, the specific gravity increases with an increase in the weight percentage of the filler in all compositions. However, the relative increase in the specific gravity of 24-nm $Ca_3(PO_4)_2$ is highest; it is 1.39. The increase is higher in the case of bigger particles for all weight percentages. Commercial $CaSO_4$ shows an increase in the specific gravity with an increase in the filler content, which is greater than the reduced size of the nanoparticles in the composites. This is due to the formation of spherulites in greater numbers for a smaller nanosize, whereas the formation of spherulites is less for a bigger size. Thus, the nanoparticles act as nanospacers more efficiently at a smaller size, and this results in a lower density in comparison with a bigger size. Petrovic et al.[21] studied the specific gravity of a polyurethane–SiO_2 system. They found that the density of the samples increased with an increase in the filler concentration for micrometer and nanosize fillers, whereas nanosize SiO_2 showed less of an increase in the specific gravity in comparison with micrometer-size SiO_2.

Effect of nano-$CaSO_4$ and nano-$Ca_3(PO_4)_2$ with variations in the weight percentage and reductions in the nanosize on the mechanical properties

Tensile strength

Figure 7 shows the effect of the variation of the size of $CaSO_4$ and $Ca_3(PO_4)_2$ on the tensile strength of the PP matrix. An increase in the tensile strength has been recorded up to 0.2 wt % nano-$CaSO_4$. Subsequently, it decreases with an increase in the addition of nanoparticles beyond 0.2 wt %. This is due to the greater surface area for smaller nanoparticles, which results in disordered exfoliation at a higher weight

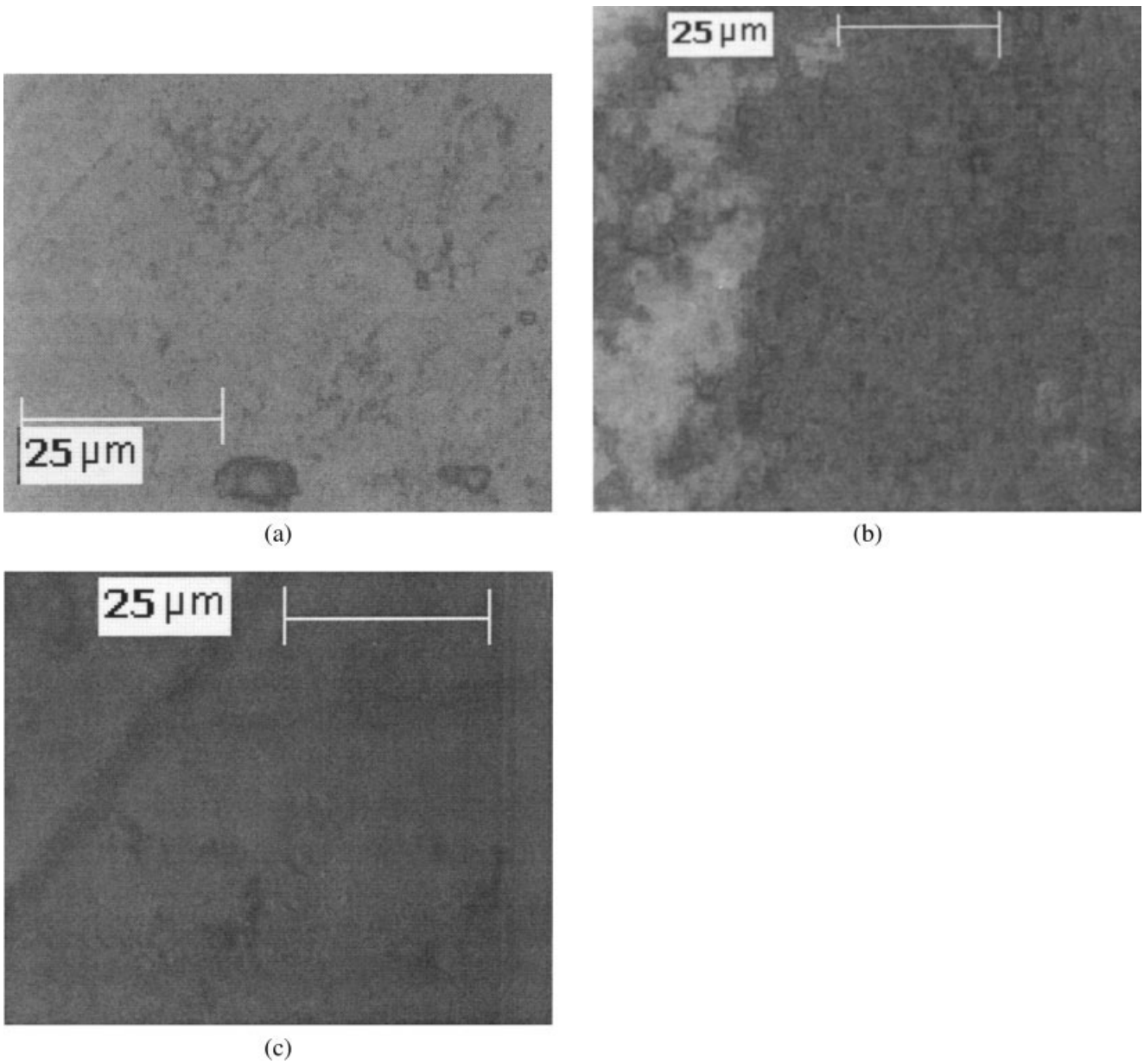

Figure 3 Optical micrographs (400×) of (a) virgin PP, (b) a 0.1 wt % 13-nm $Ca_3(PO_4)_2$/PP composite, and (c) a 0.5 wt % 13-nm $Ca_3(PO_4)_2$/PP composite.

percentage of the filler loading, whereas commercial $CaSO_4$, which is micrometer-size, does not show disordered exfoliation. Hence, the addition of commercial $CaSO_4$ shows a marginal but continuous increase in the tensile strength. The tensile strength has been recorded as 29 MPa at a 0.2 wt % loading of commercial $CaSO_4$, whereas the loading of 12- and 22-nm $CaSO_4$ shows 46 and 35 MPa, respectively. This is quite comparable to the pristine matrix, and it is quite lower (29 MPa) than that of the reduced nanosize (12-nm) composite. Unlike $CaSO_4$, 13-nm $Ca_3(PO_4)_2$ shows a continuous increase with an increase in the amount from 0.1 to 0.5 wt %, which is not observed for bigger (24-nm) $Ca_3(PO_4)_2$. Overall, the reduction in the nanosize gives a higher increase in the tensile strength for both $CaSO_4$ and $Ca_3(PO_4)_2$. This is due to the higher nucleation and local orientation of matrix molecules. The variation in the tensile strength with an increase in the amounts of the fillers is due to the morphology of the particles and the sizes of the fillers. $CaSO_4$ is a needlelike structure, and $Ca_3(PO_4)_2$ has a spherical structure that imparts the tensile properties.[11,15]

Elongation at break

The elongation at break (%) decreases with an increase in the weight percentage of the filler, except for 13-nm $Ca_3(PO_4)_2$ in the composites (Fig. 8). Commercial $CaSO_4$ shows a sharp decrease in comparison with the nanosize composites. This is due to the

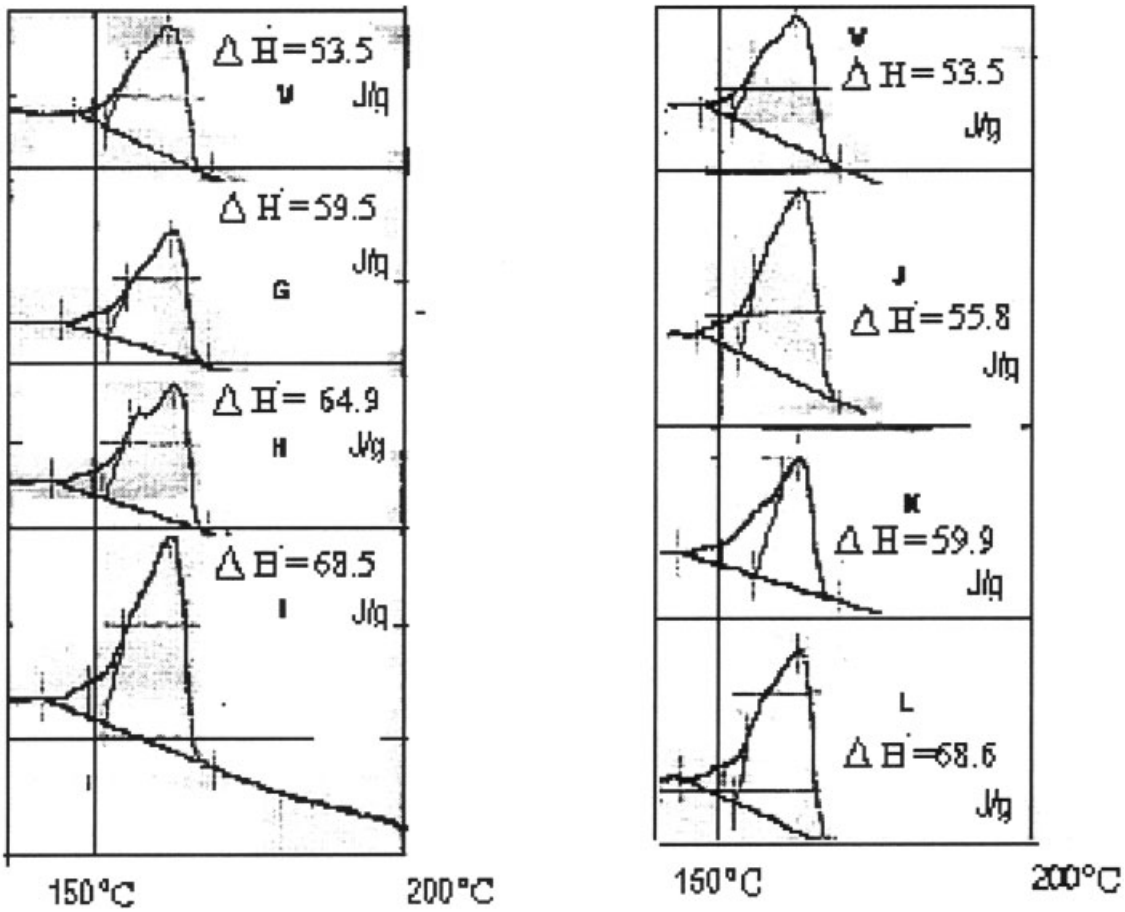

Figure 4 DSC thermograms of nano-$CaSO_4$/PP composites: (V) virgin PP; (G) 0.5, (H) 0.3, and (I) 0.1 wt % 12-nm $CaSO_4$/PP composites; and (J) 0.5, (K) 0.3, and (L) 0.1 wt % 22-nm $CaSO_4$/PP composites (ΔH = heat of fusion).

fact that the micrometer-size particles imply higher brittleness. The decrease in the flexibility is more prominent in the commercial filler than the nanosize fillers, so the flexibility can be kept unaffected with a reduction in the nanosize at a higher loading. The difference in the elongation at break (%) for the reduced nanosize composite is higher in comparison with the bigger size. As the weight percentage of the filler increase for the reduced nanosize, the shearing of the chains is reduced. The reduction in the nanosize brings the chains closer to the nucleus, at which the formation of spherulites is more in comparison with the bigger size. Therefore, chain relaxation increases with a decrease in the particle size, and this causes an increase in the elongation at break (%). On comparing all results, we can visualize the structural effect on the mechanical properties. The reduced nanosize of $CaSO_4$ and $Ca_3(PO_4)_2$ is approximately the same, that is, 12 and 13 nm, respectively; however, the structures are different, as mentioned earlier in this article. A spherical structure gives a higher increase in the chain shearing, and so the elongation increases with an increase in the loading of $Ca_3(PO_4)_2$ in comparison with $CaSO_4$ up to a certain extent.

Young's modulus

Upon the addition of nano-$CaSO_4$, the increase in Young's modulus is more pronounced for a bigger particle size than the reduced size (Fig. 9). This is due to the fact that the bigger particle size of the filler hinders the mobilization of the matrix molecules, and this leads to higher rigidity. More brittleness can be observed for commercial $CaSO_4$. A smaller increase in Young's modulus can be observed for smaller nanosizes, and this is due to the higher mobilization of the matrix molecules. The optimum value of Young's modulus for a higher nanosize (22 nm) is 59.4 MPa for a 0.3 wt % filler loading. The optimum value of the reduced nanosize (12 nm) is 52.60 MPa for the same weight percentage of the filler loading, but a continuous increase can be observed for commercial $CaSO_4$. The same effect, like that of commercial $CaSO_4$, can also be observed for bigger nanosizes of $Ca_3(PO_4)_2$. This might be due to structural differences in the two fillers: nano-$CaSO_4$ has a needlelike structure, whereas $Ca_3(PO_4)_2$ is spherical. As the particle size of $CaSO_4$ increases, the aspect ratio of the particle decreases; hence, the commercial $CaSO_4$ shows a trend like that of

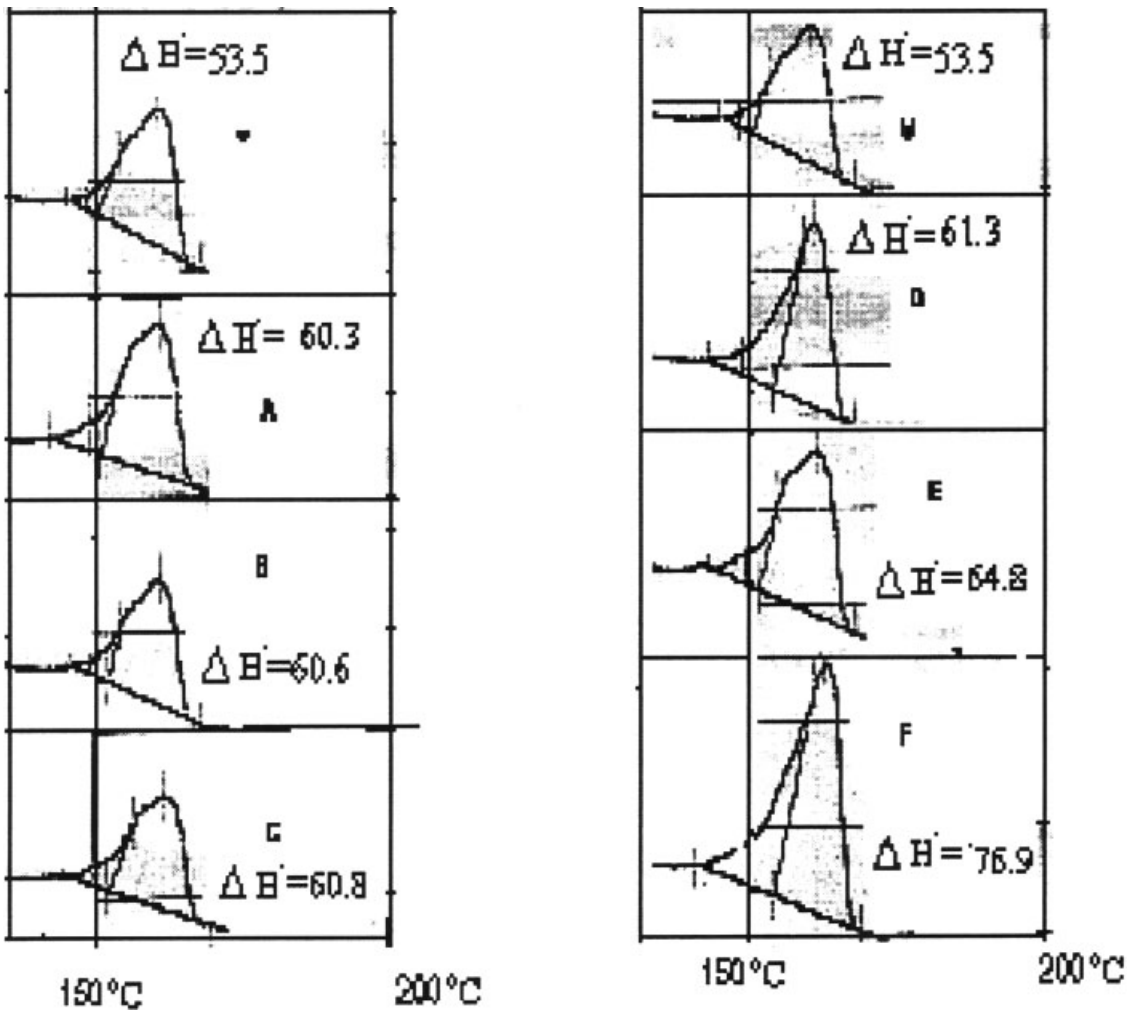

Figure 5 DSC thermograms of nano-$Ca_3(PO_4)_2$/PP composites: (V) virgin PP; (A) 0.5, (B) 0.3, and (C) 0.1 wt % 13-nm $Ca_3(PO_4)_2$/PP composites; and (D) 0.5, (E) 0.3, and (F) 0.1 wt % 24-nm $Ca_3(PO_4)_2$/PP composites (ΔH = heat of fusion).

$Ca_3(PO_4)_2$. The optical micrographs (400×) of virgin PP, 0.1 and 0.5 wt % 13-nm $Ca_3(PO_4)_2$/PP composites, and 0.1 and 0.5 wt % 12-nm $CaSO_4$/PP composites are shown in Figures 4 and 5. The reduction in the nanosize clearly results in the formation of smaller spherulites with a uniform dispersion in comparison with larger nanosize particles in the composites. This is also strengthened by our earlier work,[17] in which

TABLE I
Peak Temperatures and Heats of Fusion for Different Compositions of Various Nanosizes of $CaSO_4$ and $Ca_3(PO_4)_2$ in PP

Composition	Peak temperature (°C)	Heat of fusion (J/gm)	Crystallinity (%)
Virgin PP	162.161	53.494	25.88
$CaSO_4$, 12 nm, 0.1%	162.965	68.531	33.15
$CaSO_4$, 12 nm, 0.3%	163.296	64.887	31.39
$CaSO_4$, 12 nm, 0.5%	162.540	59.515	28.79
$CaSO_4$, 22 nm, 0.1%	162.638	68.576	33.17
$CaSO_4$, 22 nm, 0.3%	162.596	59.923	28.99
$CaSO_4$, 22 nm, 0.5%	162.765	55.798	26.99
$Ca_3(PO_4)_2$, 13 nm, 0.1%	162.407	61.339	29.67
$Ca_3(PO_4)_2$, 13 nm, 0.3%	162.085	60.309	29.45
$Ca_3(PO_4)_2$, 13 nm, 0.5%	162.600	60.002	29.02
$Ca_3(PO_4)_2$, 24 nm, 0.1%	163.665	76.879	37.19
$Ca_3(PO_4)_2$, 24 nm, 0.3%	162.601	64.800	31.37
$Ca_3(PO_4)_2$, 24 nm, 0.5%	162.695	61.244	29.63

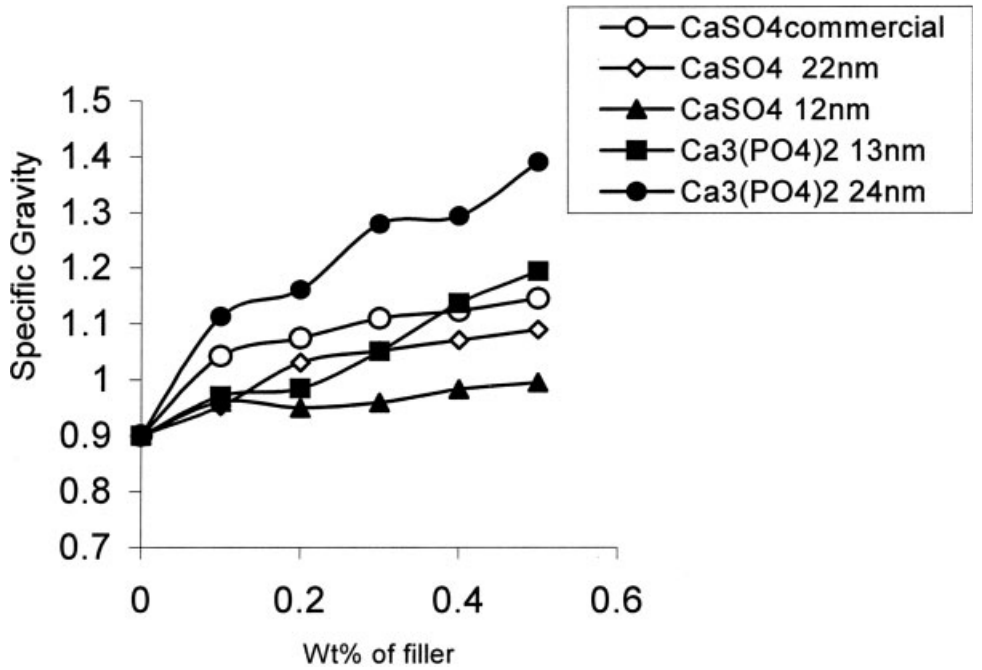

Figure 6 Comparison of the effects of different nanosizes on the specific gravity of nano-$CaSO_4$/PP and nano-$Ca_3(PO_4)_2$/PP composites.

the formation of a greater number of spherulites was observed with a reduction in the nanosize of $CaCO_3$. The spherulites of bigger nanoparticles grow for a longer period, whereas they grow for a shorter period for smaller nanoparticle. In the case of bigger nanoparticles, unlike the smaller nanoparticles, the number of particles is lower for restricting the growth of spherulites by the formation of new spherulites. Hence, the growth of the spherulites affects the ultimate mechanical properties of the polymer matrix.

Hardness

Figure 10 shows the results of the Shore D hardness for composites with different nanosizes of $CaSO_4$ or $Ca_3(PO_4)_2$ or commercial $CaSO_4$. The hardness increases with the decreasing size of $CaSO_4$. The commercial $CaSO_4$ shows minimum hardness in comparison with the nanosizes. However, it shows a continuous increase in the hardness with an increase in the amount of commercial $CaSO_4$ in the composites. Such an increase is limited at 0.2 wt % for 12-nm $CaSO_4$ and 0.3 wt %

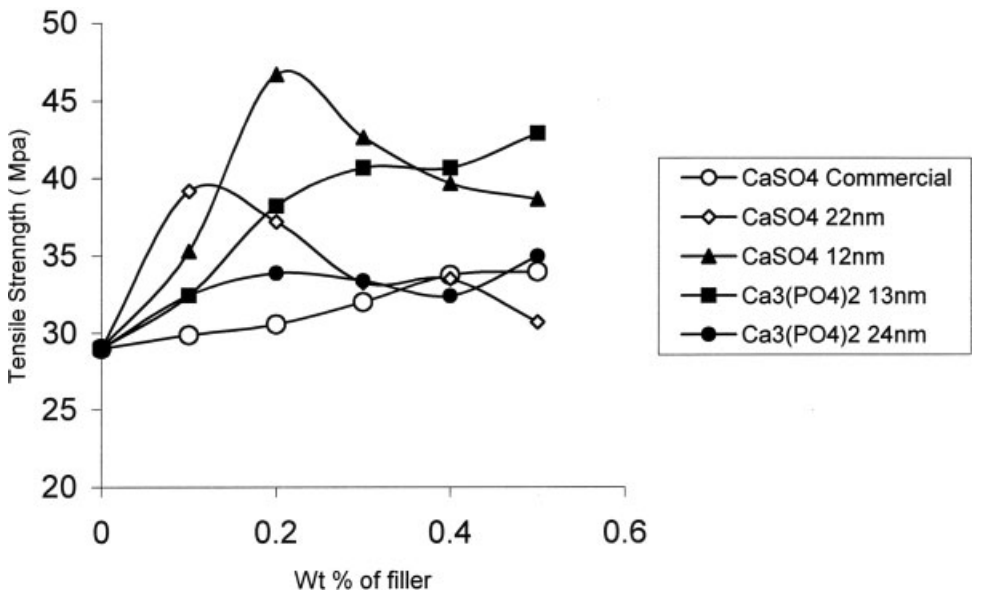

Figure 7 Comparison of the effects of different nanosizes on the tensile strength of nano-$CaSO_4$/PP and nano-$Ca_3(PO_4)_2$/PP composites.

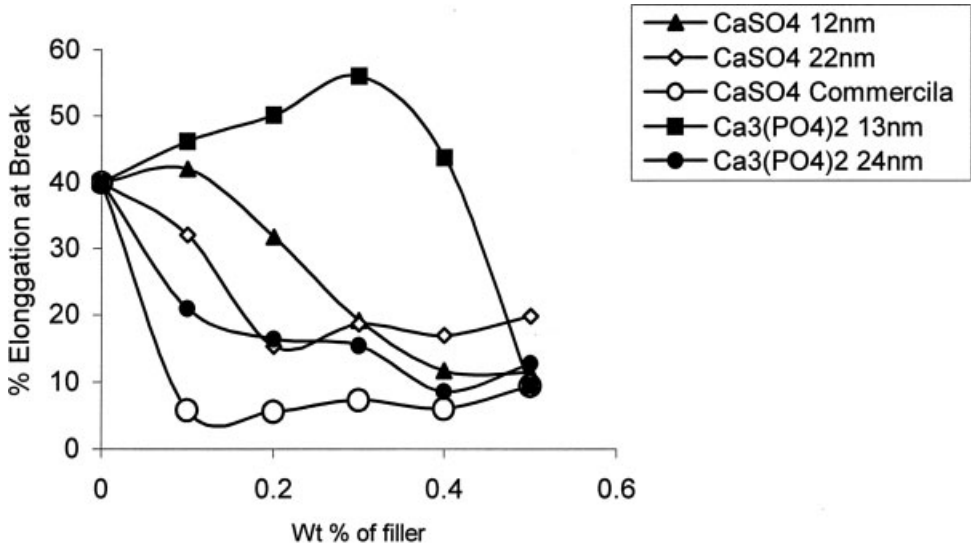

Figure 8 Comparison of the effects of different nanosizes on the elongation at break (%) of nano-$CaSO_4$/PP and nano-$Ca_3(PO_4)_2$/PP composites.

22-nm $CaSO_4$, and above these percentages, a decrease in the hardness is recorded. Unlike $CaSO_4$, $Ca_3(PO_4)_2$ shows greater hardness for bigger nanosizes. However, the hardness increases with an increase in the weight percentage of the filler loading at smaller nanosizes (13 nm) of $Ca_3(PO_4)_2$, although 24-nm $Ca_3(PO_4)_2$ shows an increase in hardness up to a 0.3 wt % loading in the composites. These results also strengthen the view that the same concentration of smaller nanoparticles forms a greater number of spherulites, and this creates a greater extent of local crystallization but a decrease in the overall crystallization. Hence, smaller nanoparticles of $CaSO_4$, which are needlelike in structure and have a greater aspect ratio, are oriented in the same direction that causes greater hardness.

Flame-retardancy behavior of nano-$CaSO_4$/PP and nano-$Ca_3(PO_4)$/PP

It can be observed from the results the that burning time increases with an increase in the filler loading of nano-$Ca_3(PO_4)_2$. Similarly, the rate of burning decreases more pronouncedly with a reduction in the nanosize (Fig. 11). The values obtained for the rate of burning are 141 and 96 s/mm for 0.4 wt % loadings of $Ca_3(PO4)_2$ of 13- and 24-nm sizes, respectively, but the maximum values are observed at 131 and 134 s/mm for 0.3 wt % commercial and 22-nm $CaSO_4$, respectively. The rate of the conduction of heat decreases and the rate of the absorption of heat increases with a decrease in the particle size of the filler. Therefore, the

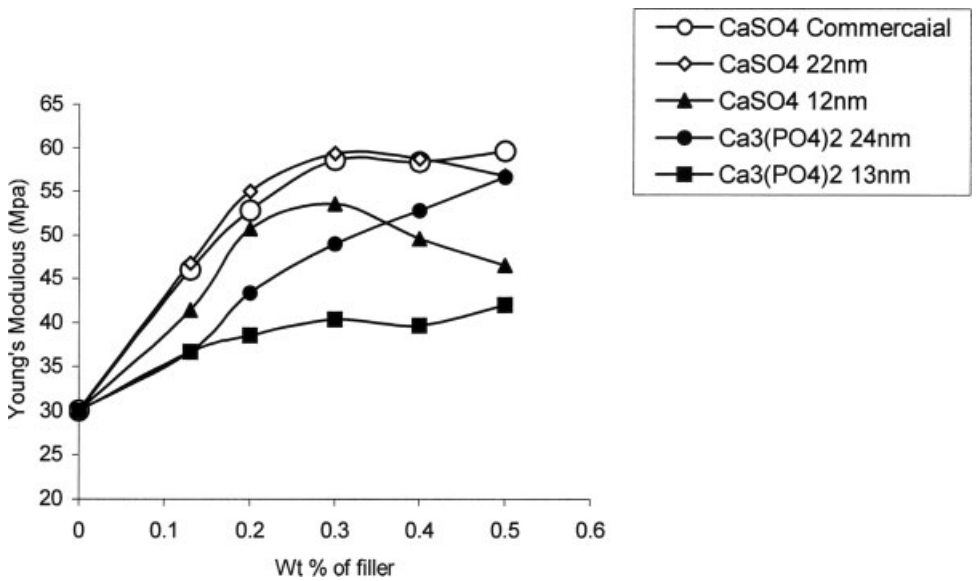

Figure 9 Comparison of the effects of different nanosizes on Young's modulus of nano-$CaSO_4$/PP and nano-$Ca_3(PO_4)_2$/PP composites.

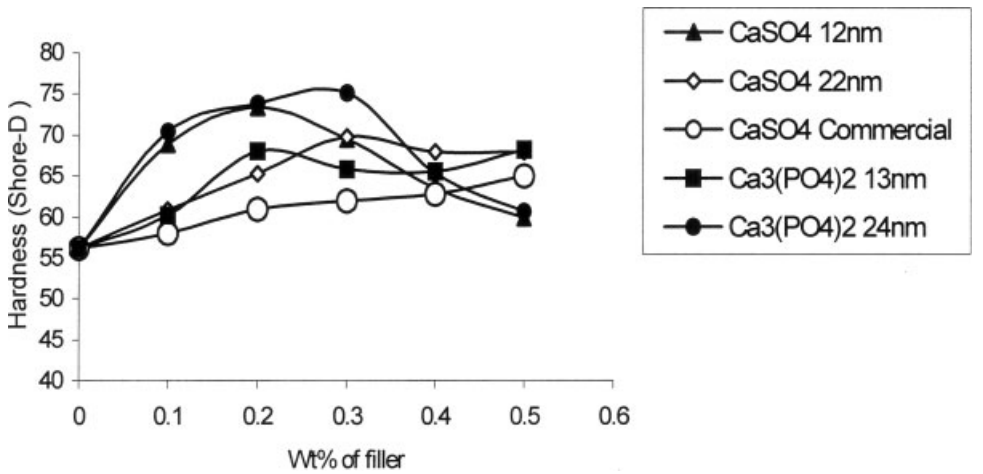

Figure 10 Comparison of the effects of different nanosizes on the hardness (Shore D) of nano-$CaSO_4$/PP and nano-$Ca_3(PO_4)_2$/PP composites.

time required for burning decreases with increases in the amount of the filler in the case of a bigger particle size, whereas the time required for burning the composites increases with an increase in the concentration of smaller nanoparticle fillers. A continuous increase in the time of burning can be observed for 12-nm nano-$CaSO_4$, and the trend of decreasing is greater for commercial $CaSO_4$ than the nanosizes.

Like $Ca_3(PO_4)_2$, nano-$CaSO_4$ shows the same behavior for the rate of burning, However, the required burning time is greater for commercial and 24-nm $CaSO_4$ (0.3 wt %), although 12-nm $CaSO_4$ shows an increase in the burning time with an increase in the filler loading up to 0.5 wt %. The longest burning time is required upon the filler addition of up to 0.4 wt % 13-nm $Ca_3(PO_4)_2$. Considering the overall results, we can conclude that the uniform dispersion of nanoparticles, the absorption of a higher amount of energy, and the charring nature of $Ca_3(PO_4)_2$ are responsible for enhancing the burning time of the samples.

Vicat softening temperature (VST)

Upon the addition of different weight percentages of the nanofillers, an increase in VST can be observed up to a certain level, and a further decrease can be observed in both cases (Fig. 12). This is due to the greater interaction of the filler particles (acting as spacer) and proper orientation of the matrix molecules. The maximum VST temperatures are 115, 121, and 125°C for 12-nm, 22-nm, and commercial $CaSO_4$,

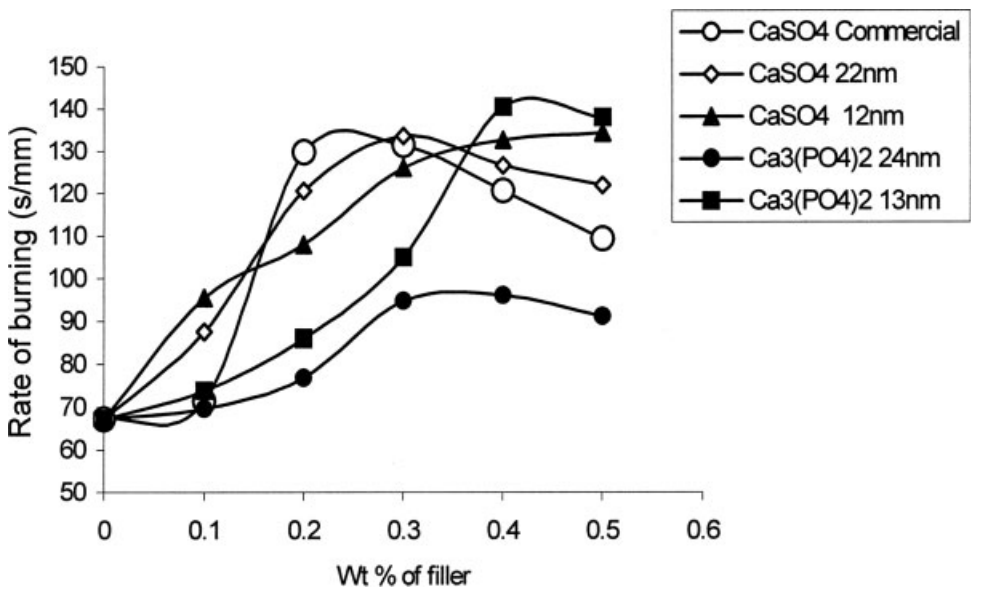

Figure 11 Comparison of the effects of different nanosizes on the rate of burning of nano-$CaSO_4$/PP and nano-$Ca_3(PO_4)_2$/PP composites.

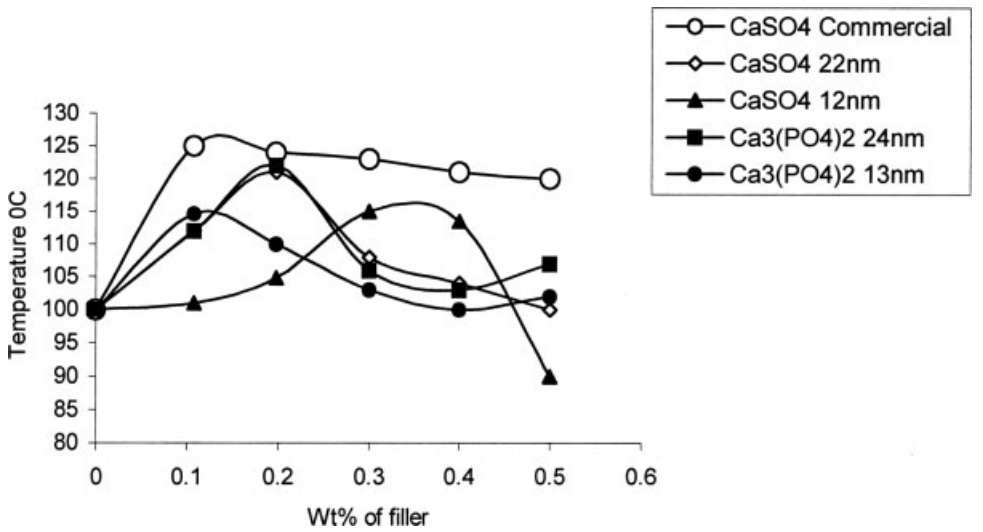

Figure 12 Comparison of the effects of different nanosizes on VST of nano-$CaSO_4$/PP and nano-$Ca_3(PO_4)_2$/PP composites.

respectively. The maximum VST is more pronounced for the smaller nano-$Ca_3(PO_4)_2$ particles. The highest values are 115°C for the 0.2 wt % 13-nm filler and 122°C for the 0.1 wt % 24-nm filler. These results show a decrease in the degree of crystallinity with an increase in the amount of the filler and a reduction in the size of the filler. As discussed earlier in this article, fewer spherulites are formed when the spherulites are bigger. The size of the spherulite is solely responsible for the increase in the Vicat temperature. Therefore, commercial $CaSO_4$/PP composites show much higher temperatures for softening at a specific load.

CONCLUSIONS

A change in phase from α to β has been observed with FTIR spectra and DSC thermograms, which show multiple melting peaks of nano-$Ca_3(PO_4)_2$/PP and nano-$CaSO_4$/PP composites. A reduction in the nanosize leads to faster nucleation by the formation of spherulites, as observed in optical micrographs; this increases the mechanical properties, but disordered exfoliation at higher weight percentages of the filler loading in the composites decreases the mechanical properties. The nanoparticles behave as spacers, so increases in the specific gravity are smaller in smaller nanoparticle filled PP composites. A higher cooling rate is possible with a decrease in the nanosize and an increase in the filler content. This effect is due to the uniform dispersion of nanoparticles in the matrix, which leads to a uniform absorption of energy.

Thanks are due to Jain Irrigation System (Jalgaon) for extending its support for the preparation of the composite sheets.

References

1. Avella, M.; Errico, M.; Martuscelli, E. Nanoletters 2001, 1, 213.
2. Hambir, S.; Balukh, N.; Kodgire, P.; Kalgaonkar, R.; Jog, J. P. J Polym Sci Part B: Polym Phys 2001, 39, 446.
3. Ou, C. F. J Appl Polym Sci 2003, 89, 3315.
4. Fornes, T. D.; Yoon, P. J.; Keskkula, H.; Paul, D. R. Polymer 2001, 42, 9929.
5. Jana, S. C.; Jain, S. Polymer 2001, 42, 6897.
6. Lien, S.; Hsu, C.; Chang, K.-C. Polymer 2002, 42, 4097.
7. Zedra, A. S.; Lesser, A. J. J Polym Sci Part B: Polym Phys 2001, 39, 1137.
8. Sanchez, C.; Babonneau, F.; Banse, F.; Doeuff Barboux, S.; Ribot, F. Mater Sci Forum 1994, 152, 313.
9. Wang, H.; Gao, L.; Li, W.; Li, Q. Nanostruct Mater 1999, 11, 1263.
10. Wang, W. D.; Wang, Y. B.; Liu, T.; Guo, L.; Tao, Y. Nanostruct Mater 1999, 11, 487.
11. Radhakrishnan, S.; Saujanya, C. J Mater Sci 1998, 33, 1069.
12. Godvski, Y. D. Adv Polym Sci 1999, 119, 79.
13. Sherman, L. M. Plast Technol 1999, 45, 53.
14. Atozi, M.; Rundle, J. Chem Phys 1958, 29, 1306.
15. Saujanya, C.; Radhakrishanan, S. Polymer 2001, 42, 6723.
16. Mishra, S.; Sonawane, S. H.; Singh, R. P.; Bendale, A.; Patil, K. J Appl Polym Sci 2004, 94, 116.
17. Mishra, S.; Sonawane, S. H.; Singh, R. P. J Polym Sci Part B: Polym Phys 2004, 43, 107.
18. Herist, C.; Mathieu, J. P.; Vogels, C.; Rulmont, A.; Cloots, R. J Cryst Growth 2003, 249, 321.
19. Wang, K. H.; Koo. C. M.; Chung, I. J. J Appl Polym Sci 2003, 89, 2131.
20. Jog, J. P.; Priya, L. J Appl Polym Sci 2003, 89, 2036.
21. Petrovic, Z. S.; Javin, I.; Waddon, A.; Banhegyi, G. J Appl Polym Sci 2000, 76, 133.